RSC Advances

PAPER

View Article Online
View Journal | View Issue

Cite this: *RSC Adv.*, 2016, **6**, 60683

Magnetic nanoparticles of Ni/NiO nanostructured in film form synthesized by dead organic matrix of yeast

Marcia Regina Salvadori,*[a] Rômulo Augusto Ando,[b] Diego Muraca,[c] Marcelo Knobel,[c] Cláudio Augusto Oller Nascimento[d] and Benedito Corrêa[a]

An innovative sustainable protocol of nanobiotechnology has been developed to synthesize Ni/NiO magnetic nanoparticles, nanostructured in film form, through a dead organic matrix of the yeast *Rhodotorula mucilaginosa*, which was isolated from the Amazon region. It is a synergistic strategy that utilizes green technology, thus minimizing environmental impact and reducing costs. The best conditions for the adsorption of the metal through the dead organic matrix and subsequent synthesis of the nanoparticles were monitored by analyzing the biosorption of nickel by the yeast. The structural characteristics of the film-forming nanoparticles were investigated *via* high-resolution transmission electron microscopy (HRTEM), atomic force microscopy (AFM), X-ray photoelectron spectroscopy (XPS), and infrared spectroscopy (FTIR). The magnetic properties of the nanoparticles produced by the dead organic matrix were determined in a superconducting quantum interference device (SQUID). Results indicate that the Ni/NiO nanoparticles are mainly spherical, with an average size of 5.5 nm, present magnetic properties, synthesized extracellularly and involve the proteins of the yeast, which probably confer organization in the film form. Such natural bioprocess suggests a rational protocol strategy as a template for the industrial-scale synthesis of magnetic nanoparticles of metals from the dead organic matrix of yeast and also provides a possible green system of nanobioremediation of metals from wastewater.

Received 19th March 2016
Accepted 6th June 2016

DOI: 10.1039/c6ra07274g

www.rsc.org/advances

Introduction

Nanotechnology arises from the chemical, physical and biological sciences, wherein novel approaches are being developed to explore and manipulate single atoms and molecules. The synthesis of pure metal nanoparticles (NPs) is challenging due to the inherent difficulty in controlling the oxidation of the metallic surface, which is mainly due to its high surface chemical potential.[1] This phenomenon, however, sometimes results in the formation of an important type of nanostructure known as "core–shell" NPs.[2] In recent years, these NPs have received remarkable attention,[3,4] in particular Ni/NiO NPs, because of their capacity for use in histidine-tagged proteins,[5] catalyzing the reduction of CO_2,[6] and as an anode material for replacing the current ceramic anode materials in fuel cells, batteries and capacitors.[7]

Bi-magnetic core/shell nanoparticles produce effects such as tunable blocking temperatures, large exchange bias tailored coercivities (spring magnets), high resonance fields or proximity effects and two-stage magnetization reversal.[8] Some of these properties have applications in diverse fields such as magnetoresistive devices (enhanced magnetoresistance after field cooling),[9] magnetic recording (enhanced blocking temperature),[10] hard magnets (increased energy products),[11] improved magnetocaloric materials,[12] biomedical applications,[13] magnetic resonance imaging,[14] and shielding (superior microwave absorption).[15]

Usually, NPs are produced *via* physical and chemical methods.[16,17] The introduction of microorganisms in the nanosynthesis of NPs is an emerging multidisciplinary technique of nanotechnology and biotechnology and has appeared as a sustainable and simple alternative to more complex physical and chemical synthetic procedures to obtain nanomaterials. The insertion of nickel into the environment has increased considerably in recent years, mainly due to industrial pollution from activities such as mining and smelting.[18] Microorganisms such as fungi play an important role as "nanofactories" in the bioremediation of toxic metals (such as

[a]*Department of Microbiology, Biomedical Institute II, University of São Paulo, São Paulo, São Paulo, 05508000, Brazil. E-mail: mrsal@usp.br*

[b]*Department of Fundamental Chemistry, Institute of Chemistry, University of São Paulo, São Paulo, São Paulo, 05508000, Brazil*

[c]*Gleb Wataghin Physics Institute, University of Campinas (UNICAMP), Campinas, São Paulo 13083970, Brazil*

[d]*Department of Chemical Engineering, Polytechnic, University of São Paulo, São Paulo, São Paulo, 05508000, Brazil*

nickel) through the reduction of metal ions.[19] Fungi have several advantages over other microorganisms for NPs synthesis because most fungi species show biomass with easy handling, require simple nutrients, and possess a high cell wall-binding capacity.[20,21]

Therefore, there is an increasing tendency to develop green chemistry synthesis for the biosynthesis of nickel NPs as an option to chemical and physical methods. The live biomass of several fungi genera has been shown to be able to synthesize metal NPs, such as gold, silver, platinum, and palladium NPs,[22] for example AuNPs synthesized by the yeast *Pichia jadinii* (formerly *Candida utilis*),[23] *Saccharomyces cerevisiae* isolated from baker's yeast (AgNPs),[24] tropical marine yeast *Yarrowia lipolytica* (Au NPs),[25] yeast *Torulopsis* sp., which is capable of synthesizing nanoscale PbS nanocrystallites,[26] yeast *Schizosaccharomyces pombe* (CdS NPs),[27] and yeast MKY3 (Ag NPs).[28] However, there are few reports using dead fungal biomass for the synthesis of metal NPs.[29–33] Recently, we described the use of the dead biomass of the yeast *Rhodotorula mucilaginosa* (*R. mucilaginosa*), which was isolated from the wastewater of a mine in the Amazon region, for the production of metallic copper NPs intracellularly.[30] There are reports on the use of magnetically modified yeast for the biosorption of toxic metals.[34] However, in this present study, we explore for the first time the potential of a dead organic matrix of yeast (*R. mucilaginosa*) for the biosynthesis of magnetic NPs of Ni/NiO organized in film form and the concomitant uptake of metal from an aqueous solution. This environmentally sustainable production of NPs may lead to a safer design of magnetic nanomaterials and also the possible utilization of this natural process in the fast and low cost nanobioremediation of wastewater polluted with metals.

Materials and methods

Culture and storage of yeast

The yeast *R. mucilaginosa* was isolated from water collected from a pond of copper waste from the Sossego Mine, which belongs to the Vale S. A. Company located in Canãa dos Carajás, Pará, Brazilian Amazonia Region (06° 26′ S latitude and 50° 4′ W longitude). The *R. mucilaginosa* was cultured and stored in YEPD agar medium (10 g yeast extract per L, 20 g peptone per L, 20 g glucose per L and 20 g agar per L) and the media compounds were obtained from Oxoid (England).[35]

Nickel tolerance by *R. mucilaginosa*

The nickel tolerance of the yeast was determined as the minimum inhibitory concentration (MIC) using the spot plate method.[36] YEPD agar medium plates containing different nickel concentrations (50 to 3500 mg L^{-1}) were prepared and inocula of the tested yeast were spotted onto the metal and control plates (plate without metal). The plates were incubated at 25 °C for at least 5 days. The MIC is defined as the lowest concentration of nickel that inhibits visible growth of the yeast.

Adsorption for Ni/NiO NPs biosynthesis

All chemicals used were of analytical grade and were used without further purification. All dilutions were prepared in ultrapure water purified in a Milli-Q system (Millipore, Milford, MA). The nickel stock solution was prepared by dissolving $NiCl_2 \cdot 6H_2O$ (Carlo Erba, Milan, Italy) in double-deionized water. The working solutions were prepared by diluting this stock solution. The two types of cellular mass (live and dead) of the yeast *R. mucilaginosa* were prepared according to Salvadori *et al.*[30] The yeast cells were grown in 500 mL Erlenmeyer flasks containing 100 mL YEPD broth. The flasks were incubated on a rotary shaker at 150 rpm for 20 h at 27 °C and the biomass was harvested by centrifugation. Once harvested, the biomass was washed twice with double-deionized distilled water and used directly for the experiment, which corresponded to live biomass. For the production of dead biomass, an appropriate amount of live biomass was autoclaved at 120 °C. The effect of pH (2–6), temperature (20–60 °C), initial nickel concentration (25–600 mg L^{-1}), contact time (5–300 min), and agitation rate (50–250 rpm) on the uptake of nickel was investigated. These assays were optimized at the desired pH, temperature, metal concentration, contact time, agitation rate and biosorbent dose (0.15–1.0 g) using 45 mL of a 100 mg L^{-1} Ni(II) test solution in a plastic flask. After the desired contact time, the Ni(II) solution was separated from the cellular mass by vacuum filtration through a Millipore membrane and the residual metal ion concentration was determined by inductively coupled plasma optical emission spectrometry. The efficiency (R) of metal removal was calculated using eqn (1):

$$R = (C_i - C_e)/C_i \times 100 \quad (1)$$

where C_i and C_e are the initial and equilibrium metal concentration, respectively. The metal uptake capacity, q_e, was calculated using eqn (2):

$$q_e = V(C_i - C_e)/M \quad (2)$$

where q_e (mg g^{-1}) is the biosorption capacity of the biosorbent at any time, M (g) is the cellular mass dose, and V (L) is the volume of the solution.

Biosorption isotherm modeling

The Langmuir equilibrium model[37] was used to fit the Ni(II) biosorption isotherm experimental data. The linearized Langmuir isotherm model is given as eqn (3):

$$C_e/q_e = 1/(q_m \times b) + C_e/q_m \quad (3)$$

where q_m is the monolayer sorption capacity of the sorbent (mg g^{-1}), and b is the Langmuir sorption constant (L mg^{-1}).

Magnetic characterization of Ni/NiO NPs

The magnetic properties were measured on dried powder sample using a superconducting quantum interference device (SQUID) (Quantum Design MPMS XL7). Magnetization loops

were performed between −2 Tesla and 2 Tesla and temperatures from 2 K to 300 K. Zero-field-cooled (ZFC) and field-cooled (FC) magnetization measurements were carried out as follows: the sample was first cooled down from 300 K to 2 K in a zero magnetic field, then a static magnetic field of $H = 50$ Oe was applied, and ZFC was measured during warming up from 2 K to 300 K; finally the sample was cooled down to 5 K under the same field H and FC was measured during the cooled cycle.

Morphological and structural characterization of the Ni/NiO NPs

The dead cellular mass of yeast *R. mucilaginosa*, which presented a higher capacity to uptake nickel than live cellular mass, was used. The synthesis of Ni/NiO NPs by the dead organic matrix of yeast was studied at a concentration of 100 mg L^{-1} nickel(II) using the equilibrium model data. Biosynthesized Ni/NiO NPs, nanostructured in film form on the surface of the dead organic matrix of the yeast *R. mucilaginosa* were characterized as follows: samples of the dead organic matrix of yeast without nickel NPs and impregnated with nickel NPs were prepared for analyses *via* HRTEM through the fixation of the samples for 1 hour in 2.5% glutaraldehyde in 0.075 M phosphate buffer (pH 7.4), followed by 3 washes in 0.075 M phosphate buffer. After a second fixation step of 1 h in 1% osmium tetroxide, the cells were washed in distilled water. The cell pellet was subjected to dehydration with 30%, 50%, and 70% ethanol, followed by three dehydration steps in 100% ethanol. Infiltration of the resin was carried out by placing the pellet in 30% Quetol in ethanol for 1 hour, followed by 1 hour in 60% Quetol. After centrifugation, the pellet was resuspended in 100% Quetol for 4 h before polymerisation at 65 °C for 24 hours. Ultrathin sections were obtained and observed by HRTEM under a JEOL JEM 2100 microscope equipped with a LaB_6 gun, and JEM 2010 and JEOL 3010 microscopes operating at 200 kV with images recorded on a TV (Gatan ES500W) and CCD (TVips – 16MP). Infrared vibrational spectroscopy (FTIR) was used to identify the functional groups present in the biomass and to evaluate the spectral variations caused by the presence of nickel NPs. Infrared absorption spectra were obtained on a Bruker model ALPHA interferometric spectrometer. The samples were placed directly into the sample compartment using an attenuated total reflectance accessory of single reflection (ATR with a platinum-crystal diamond). Eighty spectra were accumulated for each sample, using a spectral resolution of 4 cm^{-1}. The samples of the dead organic matrix of the yeast without nickel NPs and impregnated with nickel NPs were placed on clean cover slips and maintained under vacuum desiccation overnight, and loaded onto a specimen holder. Furthermore, the samples were scanned on an AFM Icon Nanoscope V (Bruker) using the tapping mode AFM technique with an oscillating cantilever to scan the sample surface with a scan rate of 1 Hz and a silicon nitride tip with a resonance frequency of about 250 kHz. The chemical state of the nickel NPs was analyzed *via* XPS. The XPS analysis was carried out at a pressure of less than 10^{-7} Pa using a commercial spectrometer (UNI-SPECS UHV System). The Mg Kα line was used ($h\nu = 1253.6$ eV) and the analyzer pass energy was set to 10 eV. The inelastic background of the electron core-level spectra was subtracted using Shirley's method. The composition (at%) of the near surface region was determined with an accuracy of ±10% from the ratio of the relative peak areas corrected by Scofield's sensitivity factors of the corresponding elements. The spectra were fitted without placing constraints using multiple Voigt profiles.

Results

Nickel tolerance by *R. mucilaginosa*

The nickel tolerance potential of the yeast *R. mucilaginosa*, which was isolated from an ecosystem polluted by metals, of copper mine wastewater located in the Amazon region, revealed that this yeast showed a high resistance to nickel (up to 2971 mg L^{-1}) through the minimum inhibitory concentration (MIC) technique.

Influence of physicochemical factors on biosorption and sorption isotherm model

The capacity to synthesize the Ni/NiO NPs from Ni(II) in an aqueous solution was investigated as a function of the state of the cellular mass (dead and live), with a maximum uptake capacity of the metal ion of 29.4 mg g^{-1} (dead cellular mass) and 15.8 mg g^{-1} (live cellular mass). The parameters considering the Langmuir model isotherm were used to describe the Ni(II) biosorption for the two types of yeast cellular mass (Table 1). The optimum physicochemical operating conditions for nickel uptake for the two types of cellular mass were: initial pH 4.0, temperature of 30 °C, agitation speed of 150 rpm, contact time of 60 min, initial Ni(II) concentration of 100 mg L^{-1} and biosorbent dose of 0.75 g. Between the two forms of cellular mass used, the dead cellular mass was more efficient in nickel biosorption (94.77%) than the live cellular mass (85.85%).

Magnetic characterization of Ni/NiO NPs

The magnetic properties of the Ni/NiO NPs synthesized by the dead organic matrix of yeast were measured as a function of temperature, in which zero-field-cooled (ZFC) and zero-cooled (FC) measurements revealed the existence of different types of magnetic contributions. From the ZFC/FC curve measured with an applied field of 50 Oe (Fig. 1a), an irreversible behavior below $T_{irr} = 120$ K is observed (more details can be observed in the inset of Fig. 1a), whereas for temperatures above this, a reversible behavior is verified. On the other hand, below 70 K both

Table 1 Parameters of biosorption of nickel ions by dead and live cellular mass of *R. mucilaginosa* from simulation with the Langmuir model

Type of cellular mass	Langmuir model		
	q_m (mg g^{-1})	b (L mg^{-1})	R^2
Live	15.8	0.039	0.985
Dead	29.4	0.038	0.981

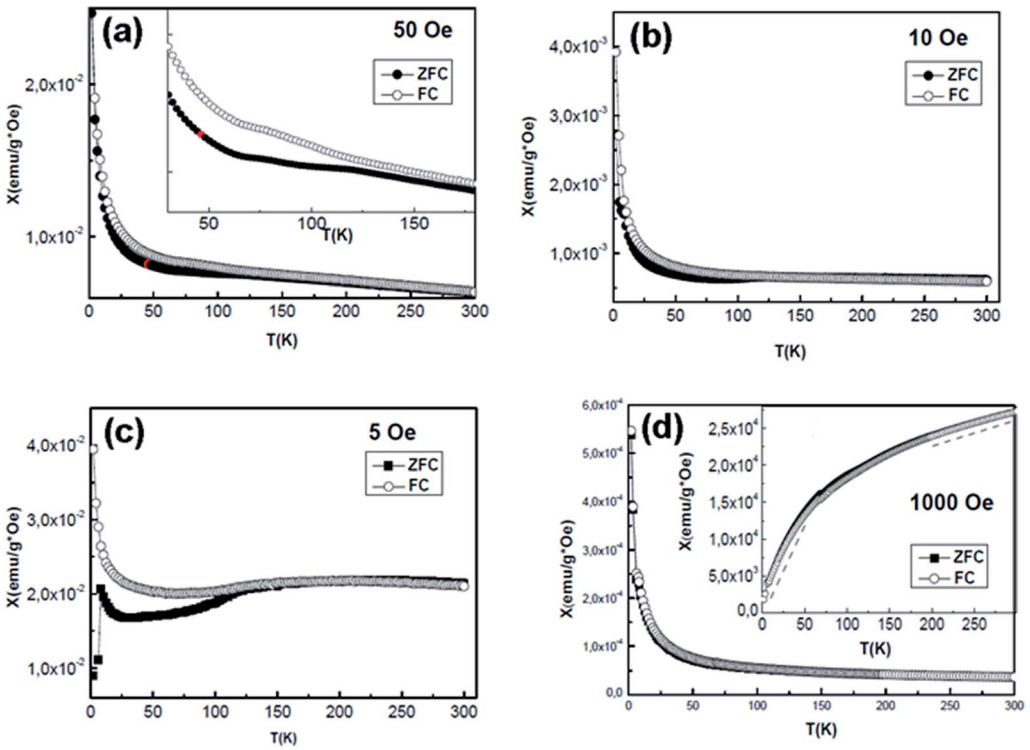

Fig. 1 ZFC/FC DC magnetic susceptibility at different applied fields: 50 Oe (a), 10 Oe (b), 5 Oe (c), and 1000 Oe (d). Inset in (a) shows in more detail the reversibility region. Inset in (d) shows the temperature dependence of the inverse of susceptibility and the dotted lines show two regions with Curie's law-like behavior.

ZFC and FC magnetization increases abruptly with a decrease in temperature. ZFC/FC measurements were performed at lower applied fields (10 Oe, Fig. 1b and 5 Oe, Fig. 1c) and at higher applied fields (1 kOe, Fig. 1d). From the low field measurements, it is observed that at very low temperatures there is a transition order, or "switching field", between 10 Oe and 5 Oe.

Magnetization loops between −2 Tesla and 2 Tesla at different temperatures between 2 K and 300 K were also measured (Fig. 2a). Non-saturated magnetization was observed at all temperatures. The inset of Fig. 2a shows in details the coercive field at three different temperatures. It is worth noting that the coercive field increases as a function of temperature (Fig. 2a, inset right). Finally, magnetization loops were measured at 2 K under the field cooling condition of 2 Tesla (Fig. 2b), from which a sort of exchange bias effect was observed (more details can be observed in the inset of Fig. 2b). Moreover, it was observed that the Ni/NiO NPs can be easily dispersed in water by simple manual agitation and easily attracted using a magnet (Fig. 2c).

Morphological and structural characterization of the Ni/NiO NPs

A detailed study of the morphological and structural characterization of the Ni/NiO NPs synthesized by the dead organic matrix of yeast (*R. mucilaginosa*), which showed organization on the film formed on its surface, was carried out due its high efficiency to uptake nickel compared with the live cellular mass. Thin cross sections of the dead organic matrix of yeast were observed using HRTEM (the control shown in Fig. 3a, which reveals the absence of NPs). After the treatment with a nickel ion solution (Fig. 3b), it was observed that the localization of the Ni/NiO NPs relative to the dead organic matrix was on the cell wall surface of the yeast (extracellular).

The HRTEM micrographs (Fig. 4) show images of the NPs that compose the film with an average size of 5.5 nm. Fig. 4 shows an agglomeration of NPs that present different contrast between the core and the shell, which could be attributed to the different oxidation states of the NPs (a). In Fig. 4 well crystallized NPs with well defined Bragg planes (b), and NPs still not well crystallized or amorphous (c) can be observed.

Analysis of the FTIR spectra (Fig. 5a and b, before and after adsorption of nickel, respectively) provided results that indicate the probable presence of proteins from the band at 1529 cm^{-1}, which was shifted to 1534 cm^{-1}, as illustrated in Fig. 5b.

Such band is assigned to N–H deformation from the amide II linkages of polypeptides or proteins,[38] which indicates that these groups act as capping agents on the surface of the particles. This may be responsible for the stabilization and structuration of the NPs in the form of a film on the dead organic matrix of *R. mucilaginosa*.

The high-resolution XPS spectra of the Ni 2p, C 1s, O 1s and N 1s core level photoemission signals after the synthesis of the Ni/NiO NPs by the dead organic matrix of *R. mucilaginosa*, which form a film on the surface of the yeast, are presented in Fig. 6. The spectra of nickel (Ni 2p) show two components (Fig. 6a),

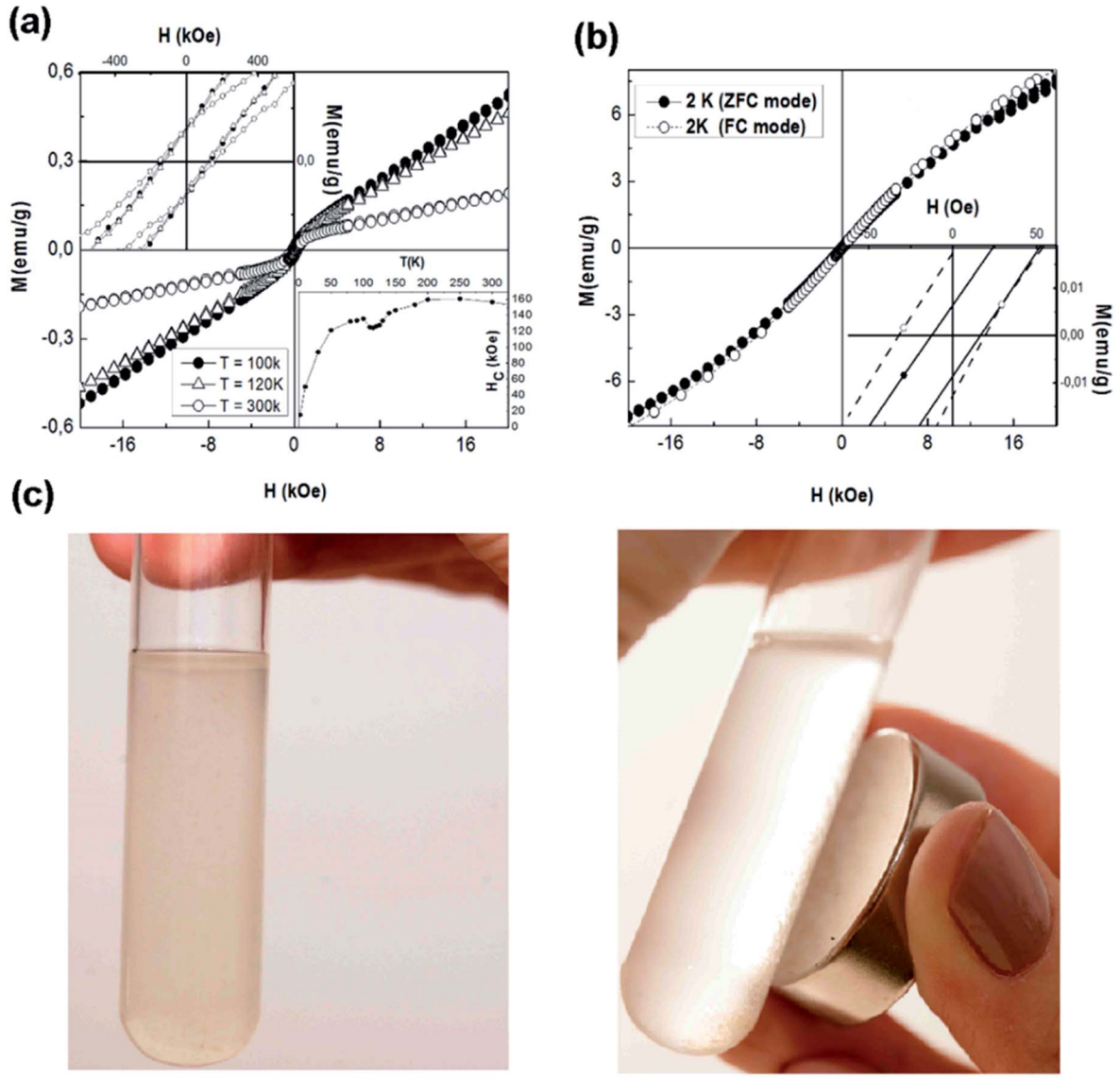

Fig. 2 (a) Magnetization loops between 2 T and −2 T at 100 K, 120 K and 300 K. Inset top left: detail of low field of the three measures. Inset down right: coercive field (H_C) obtained from magnetization loops between 2 K and 300 K; (b) magnetization loops at 2 K on ZFC and FC modes; and (c) image showing magnetic attraction of the Ni/NiO NPs.

a peak at 852.6 eV, which is characteristic of the Ni $2p_{3/2}$ level of Ni(0)[39] and a peak at 854.2 eV that corresponds to the Ni $2p_{3/2}$ level and is characteristic of NiO,[5,40,41] which verify in this study that the NPs are constituted of Ni/NiO. The components of the binding energy of the C 1s high resolution carbon spectra (Fig. 6b) were deconvoluted within four components: the peak at 285.0 eV corresponds to the hydrocarbon chains (C–H) of the cellular phase, the peak at 286.5 eV to the alpha-carbon (C–O), the peak at 288.0 eV to the carbonyl groups (C═O) and the peak at 289.1 eV to the carboxylic groups of the possible proteins bound to the NPs. In Fig. 6c, the deconvoluted spectra of oxygen (O 1s) showed a peak at 530.2 eV, which is related to the peak found in Ni 2p (NiO), and three more components, which reveal peaks at 531.4 eV (O═C), 532.5 eV (O–C) and 533.4 eV (O–C═O), and these correspond to the peaks found in the C 1s. The high resolution spectra of nitrogen (N 1s) were deconvoluted in two components at 400.0 eV (N–C) and 402.0 eV (N–O), as shown in Fig. 6d. The presence of the binding energy at 532.5 eV and 400.0 eV verified in the spectra of the core level O 1s and N 1s, respectively, corroborate with the FTIR results, which confirm the probable presence of proteins involving the Ni/NiO NPs, which act as a capping agent[42] and possibly would be involved with the nanostructuration of the Ni/NiO NPs in the film form.

AFM micrographs of the dead organic matrix of yeast were recorded to study its surface morphology.

The three-dimensional (3D) and topographic AFM images (height) of the dead organic matrix of yeast (Fig. 7a and c) show a surface structure in the absence of the nickel NPs; however, in the organic matrix in the presence of the Ni/NiO NPs (Fig. 7b and d), the organization of a film of Ni/NiO

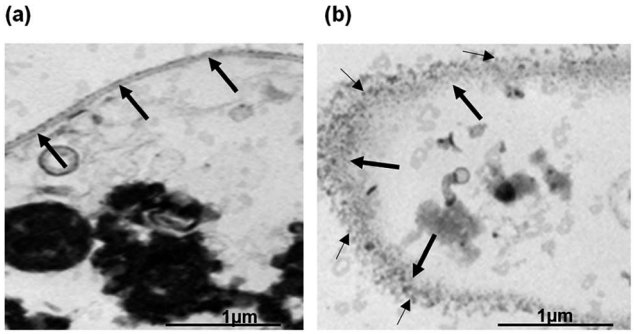

Fig. 3 HRTEM micrographs of thin cross sections of the dead organic matrix of the yeast *R. mucilaginosa*. (a) HRTEM images of the untreated (control) dead organic matrix of the yeast *R. mucilaginosa* showing the cell wall (darkest black arrows) without nanoparticles; and (b) HRTEM images showing the cell wall (darkest black arrows) with deposition of NPs extracellularly on the cell wall (lighter black arrows).

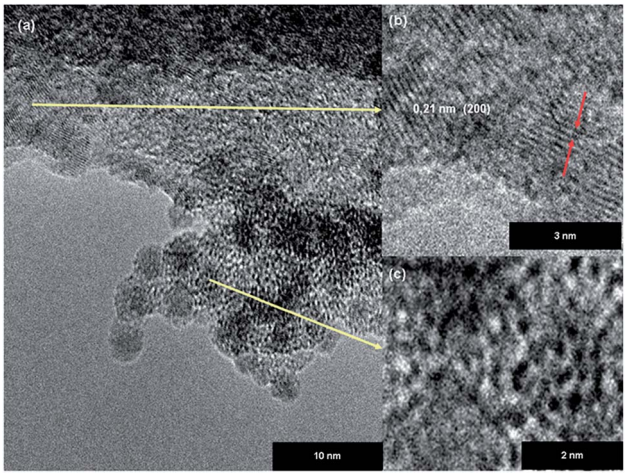

Fig. 4 HRTEM photomicrographs of the magnetic Ni/NiO NPs organized in film form on surface of the dead organic matrix (a); NP details of the selected regions, showing crystallized NPs with well defined Bragg planes (b) and amorphous NPs (c).

coating the surface of the dead organic matrix of *R. mucilaginosa* was observed.

Discussion

The biosorption technology, which is focused on the interaction between toxic metals and the binding functional groups on the cell wall structure of the microorganisms,[43] such as yeast, fungi, algae and bacteria, has been increasingly considered as a potential alternative way to remove contaminants from industrial wastewater. The high nickel tolerance by the yeast *R. mucilaginosa* (up to 2971 mg L^{-1}) is due to the mechanism of adsorption of metal ions by functional groups of the cellular wall. These groups (protein, lipids and carbohydrates) act as sorption sites of the metals, thus mediating the uptake of metal ions by the cellular wall.[44] Yeasts use some mechanisms to balance the concentration and toxicity of the metals. Moreover, the resistance mechanisms include the sequestration of heavy metals by metallothioneins through their high cysteine content and adsorption of metal ions by the cellular wall.[45,46]

The dead organic matrix of *R. mucilaginosa* revealed that it has a high adsorption capacity (29.4 mg g^{-1}) compared with other myco-adsorbents and other types of biosorbents normally used in nickel biosorption.[47–56] There are few studies reporting[29–33] the use of dead fungal cellular mass to produce metal NPs. The dead cellular mass offers advantages that are interesting for the processes of biosorption in NPs synthesis in relation to live cellular mass, such as it can be easily stored for a prolonged period of time due its minor volume and better preservation characteristics, limited toxicity, it does not need any growth media and nutrients for its maintenance, the chemically heterogeneous surface of the dead microbial cellular mass in a rapid, non-metabolically mediated process may passively sequester metals by the process of biosorption from dilute solutions,[57] and also it has a lower sensitivity to adverse operating conditions.

In Fig. 1a, a superparamagnetic (SP) behavior can be observed. The net magnetic is randomly oriented,[58] and

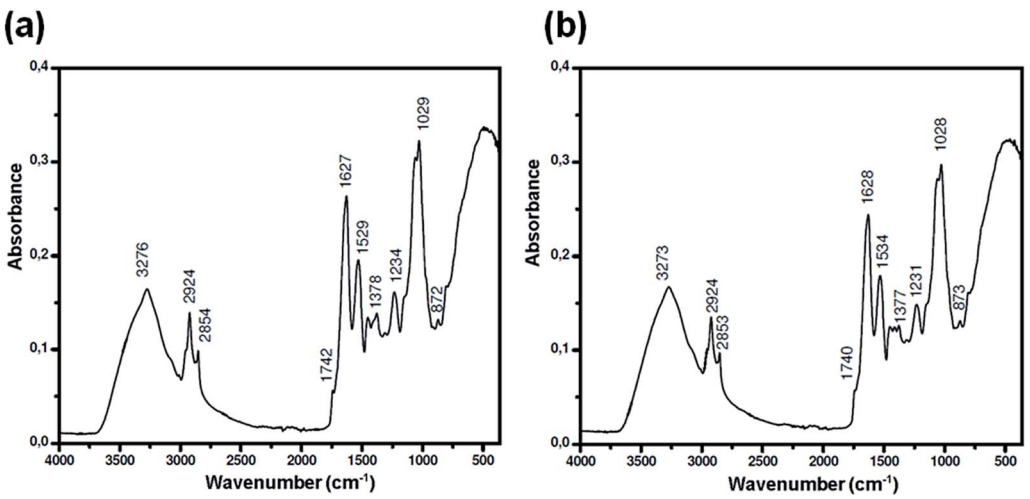

Fig. 5 FTIR spectra of the dead organic matrix of the yeast *R. mucilaginosa*. (a) Before and (b) after saturation with nickel.

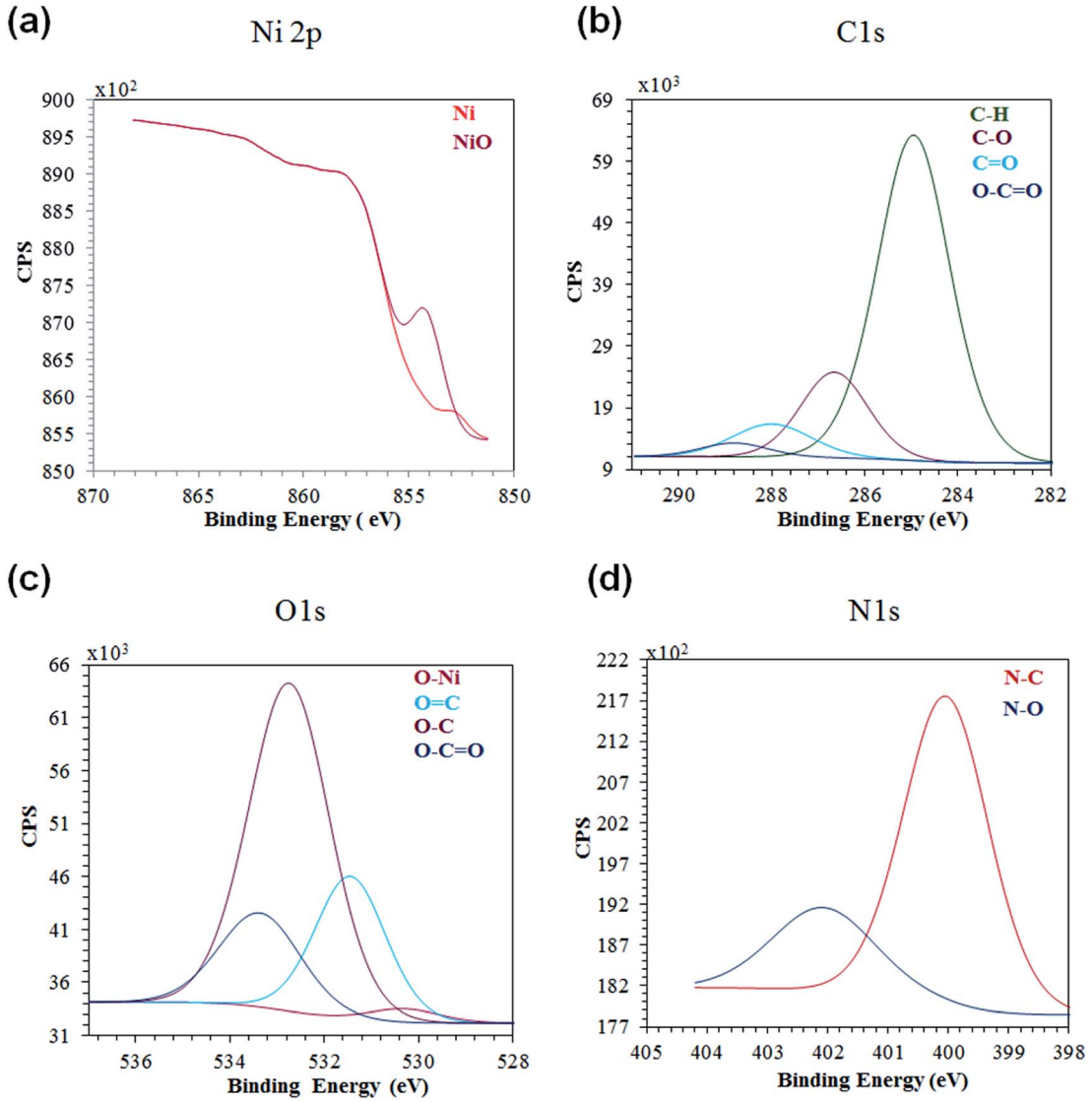

Fig. 6 High-resolution XPS spectra of the Ni/NiO NPs that compose the film biosynthesised by the dead organic matrix of the yeast *R. mucilaginosa*. (a) Ni 2p, (b) C 1s, (c) O 1s and (d) N 1s core level binding energies after the biosynthesis of the Ni/NiO NPs.

irreversibility at 120 K is also observed, which reflects the SP contribution (blocked to unblocked transition) of the Ni^0 core of the NPs. The inset of Fig. 1a shows the irreversibility region in more detail. As was previously mentioned, a transition or "switching field" was observed from the low fields (5 Oe and 10 Oe, Fig. 1b and c) to the high field (1 kOe, Fig. 1d). For low applied fields, the magnetization on the ZFC curve presents a small paramagnetic (PM) contribution. A similar behavior was reported by Estrader *et al.*[8] on another type of antiferromagnetic-core/ferrimagnetic-shell NPs. From the ZFC/FC data at high applied field and the inverse of susceptibility temperature dependence (inset), we observed two different Curie's law-type trends, one possibly associated with the SP core of the NPs and the other from the PM contribution on the NPs surface. Non-saturated magnetization was observed on the magnetization loops at all similar temperatures and the unusual behavior of the coercive field (Fig. 2a) was also observed on other soft magnetic interacting systems.[59] The exchange bias effect observed (Fig. 2b) is probably is due the coupling of the two magnetic phases on the NPs.[8]

The characterization of the morphology of the Ni/NiO NPs produced by the dead organic matrix of yeast showed an organization in the film form on its surface and electron micrographs revealed the formation of NPs extracellularly, the majority of which were spherical in shape, with an average diameter of 5.5 nm (Fig. 4). Normally, fungi are known as the organisms that produce NPs extracellularly due their enormous secretory components of extracellular protein called secretome, which secrete proteins that are involved in the ion reduction and capping of NPs.[60,61]

The mechanisms and agents involved in the extracellular synthesis of Ni/NiO NPs by the dead organic matrix of the yeast *R. mucilaginosa* are not totally known. In this study, we propose a process that comprises two-steps: in the first step,

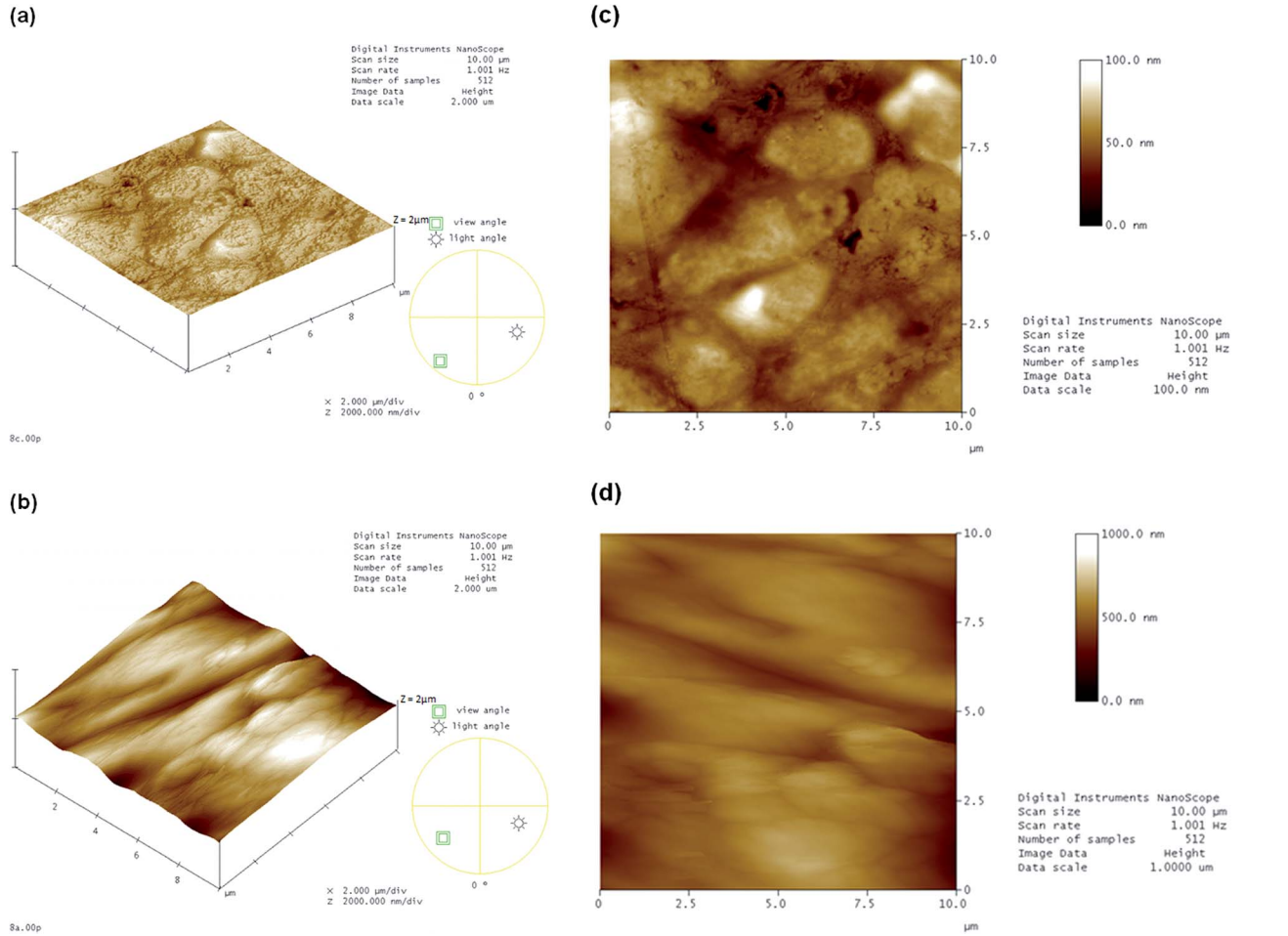

Fig. 7 AFM images of the surface of the dead organic matrix of the yeast *R. mucilaginosa*. (a) AFM image (3D) showing the dead organic matrix without Ni/NiO NPs; (b) AFM image (3D) showing the dead organic matrix after exposition of the Ni/NiO NPs, which form a film on the surface of the dead organic matrix; (c) AFM topographic image (height) showing the dead organic matrix without Ni/NiO NPs; and (d) AFM topographic image (height) showing the dead organic matrix after exposition of the Ni/NiO NPs, which form a film on the surface of the dead organic matrix.

the interaction occurs between Ni^{2+} and the amide groups located in the cell wall of the organic matrix and then subsequent bioreduction to Ni^0, which is possibly due the presence of extracellular enzymes.[61] The FTIR assays of the peptides/proteins bound to the Ni/NiO NPs indicate that they act as capping agents, which is in agreement with the findings from the XPS analysis. We may infer that the dead organic matrix of yeast possibly used extracellular proteins normally produced by fungi, as already described in the production of the NPs extracellularly.[60,61] Some yeasts of the genus *Rhodotorula* are mesophilic,[62] as well as the yeast *R. mucilaginosa* used in this study, and it is known that some mesophilic yeasts are able to produce thermostable enzymes.[63] Probably, these proteins present in the dead organic matrix of yeast are thermostable enzymes and are able to resist to the autoclaving temperature. The thermosensitive enzymes present in the dead organic matrix probably suffered denaturation during the autoclaving process thus changing the arrangement of the amino acids in the active site, changing its shape and probably causing loss of the enzyme catalytic ability.[64] Subsequently, in the second step, the oxidation of Ni^0 NPs occurs by water and oxygen present in the medium, due to the negative reduction potential of nickel. There is the formation of an oxide passivation layer forming the Ni/NiO NPs, as observed in XPS analysis.

The organization of the Ni/NiO NPs was observed by the morphological characterization in the organic matrix surface after the synthesis of the NPs in the AFM images (Fig. 7a–d), which reveal the formation of a film on the surface of the dead organic matrix of the yeast structured by the Ni/NiO NPs. There are no reports in the literature about the production of magnetic NPs of Ni/NiO by the dead organic matrix of the yeast *R. mucilaginosa*, as well as their natural structuration in film form. The presence of probable proteins surrounding the Ni/NiO NPs, which are observed by FTIR and XPS analysis, act as a capping agent in the synthesis of the Ni/NiO NPs,[42] and possibly confer their nanostructuration in the film form. However, the constitution and mechanism of action of the proteins involved in this natural process remain to be determined.

Conclusions

In summary, we demonstrate for the first time the synthesis and uptake of magnetic NPs of Ni/NiO by the dead organic matrix of the yeast *R. mucilaginosa*. In this process, it was observed that the magnetic NPs were organized in a form of a film on the organic matrix surface. This natural technique can provide a process of industrial interest due to the concomitant uptake and production of magnetic metallic NPs from toxic metals of liquid waste that can result in detoxification and safe environmental discharge. The capacity of the dead organic matrix of yeast to produce magnetic NPs of Ni/NiO nanostructured in film form can be highly promising for the sustainable synthesis of nano-metals and increase its application as a natural strategy. The clarification of the mechanisms and biomolecules involved in the synthesis of magnetic NPs of Ni/NiO and their organization in film form will be targets of our future studies.

Acknowledgements

This study was supported by the Fundação de Amparo à Pesquisa do Estado de São Paulo (FAPESP). The authors are very much thankful to the Laboratory of Photoelectron Spectroscopy (LEFE), Universidade Estadual Paulista "Júlio de Mesquita Filho" (UNESP), Araraquara, São Paulo, Brazil, by the performing the XPS analysis in this study. The authors are grateful to C2NANO-Brazilian Nanotechnology National Laboratory (LNNano) at Centro Nacional de Pesquisa em Energia e Materiais CNPEM/MCT (#14825 and 14827) and Research Proposal TEM-16976 for the use of TEM.

References

1 B. B. Nayak, S. Vitta, A. K. Nigam and D. Bahadur, *Thin Solid Films*, 2006, **505**, 109–112.
2 L. Savine, E. Bonetti, L. Del Bianco, L. Pasquini, S. Signoretti, P. Allia, M. Coisson, J. Moya, V. Selvaggini, P. Tiberto and F. Vinai, *J. Appl. Phys.*, 2002, **91**, 8593–8595.
3 B. David, N. Pizúrová, O. Schneeweiss, P. Bezdička, I. Morjan and R. Alexandrescu, *J. Alloys Compd.*, 2004, **378**, 112–116.
4 Y. Qiang, J. Antony, A. Sharma, J. Nutting, D. Sikes and D. Meyer, *J. Nanopart. Res.*, 2006, **8**, 489–496.
5 I. S. Lee, N. Lee, J. Park, B. H. Kim, Y. W. Yi, T. Kim, T. K. Kim, I. H. Lee, S. R. Paik and T. Hyeon, *J. Am. Chem. Soc.*, 2006, **128**, 10658–10659.
6 C. W. Tsai, H. M. Chen, R. S. Liu, K. Asakura and T. S. Chan, *J. Phys. Chem. C*, 2011, **115**, 10180–10186.
7 P. Poisot, S. Laruell, S. Grugeon, L. Dupont and J. M. Tarascon, *Nature*, 2000, **407**, 496–499.
8 M. Estrader, A. López-Ortega, S. Estradé, I. V. Golozovsky, G. Salazar-Alvarez, M. Vazilakaki, K. N. Trohidou, M. Varela, D. C. Stanley, M. Sinko, M. J. Pechan, D. J. Keavney, F. Peiró, S. Suriñach, M. D. Baró and J. Nogués, *Nat. Commun.*, 2013, **4**, 1–8.
9 I. Groza, R. Morel, A. Brenac, C. Beigne and I. Notin, *IEEE Trans. Magn.*, 2011, **47**, 3355–3357.
10 V. Skumryev, S. Stoyanov, Y. Zhang, G. Hadjipanayis, D. Givord and J. Nogués, *Nature*, 2003, **423**, 850–853.
11 H. Zeng, J. Li, Z. L. Wang, J. P. Liu and S. Sun, *Nano Lett.*, 2004, **4**, 3–6.
12 A. Rostamnejadi, M. Venkatesan, J. Alaria, M. Boese, P. Kameli, H. Salamati and J. M. D. Coey, *J. Appl. Phys.*, 2012, **110**, 043905.
13 E. A. Naumenko, M. R. Dzamukova, G. I. Fakhrullina, F. S. Akhatova and R. F. Fakhrullin, *Curr. Opin. Pharmacol.*, 2014, **18**, 84–90.
14 T. J. Yoon, H. Lee, H. Shall and R. Weissleder, *Angew. Chem., Int. Ed.*, 2011, **50**, 4364–4366.
15 L. Xi, Z. Wang, Y. Zuo and X. Shi, *Nanotechnology*, 2011, **22**, 045707.
16 J. P. Zhang, L. Q. Sheng and P. Chen, *Chin. Chem. Lett.*, 2003, **14**, 645–648.
17 M. G. Guzmán, J. Dille and S. Godet, *Int. J. Electr. Comput. Eng.*, 2009, **2**, 104–111.
18 M. Joho, M. Inouhe, H. Tohoyama and T. Murayama, *J. Ind. Microbiol.*, 1995, **14**, 164–168.
19 A. N. Mishra, S. Bhadauria, M. S. Gaur and R. Pasricha, *JOM*, 2010, **62**, 45–48.
20 M. A. Dias, I. C. A. Lacerda, P. F. Pimentel, H. F. De Castro and C. A. Rosa, *Lett. Appl. Microbiol.*, 2002, **34**, 46–50.
21 R. Sanghi and P. Verma, *Bioresour. Technol.*, 2009, **100**, 501–504.
22 N. C. Bigall, M. Reitzig, W. Naumann, P. Simon, K. H. van Pée and A. Eychmüller, *Angew. Chem., Int. Ed.*, 2008, **47**, 7876–7879.
23 M. Gericke and A. Pinches, *Gold Bull.*, 2006, **39**, 22–28.
24 M. Saravanan, T. Amelash, L. Negash, A. Gebreyesus, A. Selvaraj, V. Rayarand and K. Deekonda, *Int. J. Res. Pharm. Biomed. Sci.*, 2013, **4**, 822–828.
25 M. Agnihotri, S. Joshi, A. R. Kumar, S. Zinjarde and S. Kulkarni, *Mater. Lett.*, 2009, **63**, 1231–1234.
26 M. Kowshik, W. Vogel, J. Urban, S. K. Kulkarni and K. M. Paknikar, *Adv. Mater.*, 2002, **14**, 815–818.
27 C. T. Dameron, R. N. Reese, R. K. Mehra, A. R. Kortan, P. J. Carroll, M. L. Steigerwald, L. E. Brus and D. R. Winge, *Nature*, 1989, **338**, 596–597.
28 M. Kowshik, A. Shriwas, K. Sharmin, W. Vogel, J. Urban, S. K. Kulkarni and K. M. Paknikar, *Nanotechnology*, 2003, **14**, 95–100.
29 M. R. Salvadori, L. F. Lepre, R. A. Ando, C. A. O. do Nascimento and B. Corrêa, *PLoS One*, 2013, **8**, 1–8.
30 M. R. Salvadori, R. A. Ando, C. A. O. do Nascimento and B. Corrêa, *PLoS One*, 2014, **9**, 1–9.
31 M. R. Salvadori, R. A. Ando, C. A. O. do Nascimento and B. Corrêa, *J. Environ. Sci. Health, Part A: Toxic/Hazard. Subst. Environ. Eng.*, 2014, **49**, 1286–1295.
32 M. R. Salvadori, C. A. O. Nascimento and B. Corrêa, *Sci. Rep.*, 2014, **4**, 6404.
33 M. R. Salvadori, R. A. Ando, C. A. O. do Nascimento and B. Corrêa, *PLoS One*, 2015, **10**, 1–15.
34 H. Yavuz, A. Denizli, H. Gungunes, M. Safarikova and I. Safarik, *Sep. Purif. Technol.*, 2006, **52**, 253–260.

35 M. D. Machado, E. V. Soares and H. M. V. M. Soares, *J. Hazard. Mater.*, 2010, **180**, 347–353.
36 I. Ahmad, M. I. Ansari and F. Aqil, *Indian J. Exp. Biol.*, 2006, **44**, 73–76.
37 A. S. Y. Ting and C. C. Choong, *World J. Microbiol. Biotechnol.*, 2009, **25**, 1431–1437.
38 Y. X. Zhang, J. Zheng, G. Gao, Y. F. Kong, X. Zhi, K. Wang, X. Q. Zhang and D. X. Cui, *Int. J. Nanomed.*, 2011, **6**, 2899–2906.
39 R. P. Furstenau, G. McDougall and M. A. Langell, *Surf. Sci.*, 1985, **150**, 55–79.
40 P. Song, D. Wen, Z. X. Guo and T. Korakianitis, *Phys. Chem. Chem. Phys.*, 2008, **10**, 5057–5065.
41 I. Porqueras and E. Bertran, *Thin Solid Films*, 2001, **398**, 41–44.
42 V. Bansal, A. Ahamad and M. Sastry, *J. Am. Chem. Soc.*, 2006, **128**, 14059–14066.
43 M. V. Subbaiah and Y. S. Yun, *Biotechnol. Bioprocess Eng.*, 2013, **18**, 280–288.
44 S. Srivastava and I. S. Thakur, *Bioresour. Technol.*, 2006, **97**, 1167–1173.
45 D. S. Gomes, L. C. Fragoso and C. J. Riger, *Biochim. Biophys. Acta, Gen. Subj.*, 2002, **1573**, 21–25.
46 D. H. Cho and E. Y. Kim, *Bioprocess Biosyst. Eng.*, 2003, **25**, 271–277.
47 P. X. Sheng, Y. P. Ting, J. P. Chen and L. Hong, *J. Colloid Interface Sci.*, 2004, **275**, 131–141.
48 E. Malkoc, *J. Hazard. Mater.*, 2006, **137**, 899–908.
49 C. Quintelas, Z. Rocha, B. Silva, B. Fonseca, H. Figueiredo and T. Tavares, *Chem. Eng. J.*, 2009, **149**, 319–324.
50 A. T. Ozturk, T. Artan and A. Ayar, *Colloids Surf., B*, 2004, **34**, 105–111.
51 A. Shoaib, A. Naureen, F. Tanveer and N. Aslam, *Int. J. Agric. Biol.*, 2012, **14**, 831–833.
52 G. Yan and T. Viraraghavan, *Bioresour. Technol.*, 2001, **78**, 243–249.
53 Z. R. Holan and B. Volesky, *Biotechnol. Bioeng.*, 1994, **43**, 1001–1009.
54 A. Delgado, A. M. Anselmo and J. M. Novais, *Water Environ. Res.*, 1998, **70**, 370–375.
55 A. Javaid, R. Bajwa and A. Javaid, *Pak. J. Bot.*, 2010, **42**, 2105–2118.
56 T. Akar, S. Celik, A. G. Ari and S. T. Akar, *J. Chem. Technol. Biotechnol.*, 2012, **1**, 1–10.
57 M. X. Loukidou, K. A. Matis, A. L. Zouboulis and M. L. Kyriakidou, *Water Res.*, 2003, **37**, 4452–4544.
58 C. Fonseca, G. F. Goya, R. F. Jardim, R. Muccillo, N. L. V. Carreño, E. Longo and E. R. Leite, *Phys. Rev. B: Condens. Matter Mater. Phys.*, 2002, **66**, 104406.
59 W. B. Rui, Y. Hu, A. Du, B. You, M. W. Xiao, W. Zhang, S. M. Zhou and J. Du, *Sci. Rep.*, 2015, **5**, 13640.
60 K. B. Narayanan and N. Sakthivel, *Adv. Colloid Interface Sci.*, 2010, **156**, 1–13.
61 V. Girardi, C. Dieryckx, C. Job and D. Job, *Proteomics*, 2013, **13**, 597–608.
62 M. Rossi, A. Amaretti, S. Raimondi and A. Leonardi, *Biodiesel - Feedstocks and Processing Technologies*, ed. M. Stoytcheva and G. Montero, In Tech, Rijeka, Croat, 2011, vol. 9, pp. 71–92.
63 R. Leite, R. Simoes, E. Gomes and R. da Silva, *Process Biochem.*, 2007, **42**, 1101–1106.
64 G. J. Tortora, B. R. Funk and C. L. Case, *Microbiology an Introduction*, Addison Wesley Longman, California, 6th edn, 1997, vol. 5, pp. 116–117.